mater.scichina.com link.springer.com

Published online 25 May 2020 | https://doi.org/10.1007/s40843-020-1346-0
Sci China Mater 2020, 63(8): 1518–1525

SPECIAL ISSUE: Optical Gain Materials towards Enhanced Light-Matter Interactions

Facile deposition of high-quality $Cs_2AgBiBr_6$ films for efficient double perovskite solar cells

Dandan Zhao[†], Bingzhe Wang[†], Chao Liang[†], Tanghao Liu, Qi Wei, Sisi Wang, Kaiyang Wang, Zhipeng Zhang, Xiaojun Li, Shaomin Peng and Guichuan Xing[*]

ABSTRACT Lead-free double perovskite, $Cs_2AgBiBr_6$, with higher stability and lower toxicity than those of its lead counterparts, has been considered a promising alternative for next-generation photovoltaic materials. For practical applications, a facile deposition method that could be used to fabricate high-quality double perovskite films with large grain size is highly desired. However, such kind of facile method has never been established for $Cs_2AgBiBr_6$. Herein, high-quality $Cs_2AgBiBr_6$ thin films with an average grain size of approximately 0.5 μm were successfully deposited *via* a simple one-step spin-coating method by using dimethyl sulfoxide (DMSO)-*N*,*N*-dimethylformamide (DMF) mixture with optimized volume ratio as the solvent and chlorobenzene (CB) as the antisolvent. On the basis of satisfactory quality of the film, efficient (>1%) $Cs_2AgBiBr_6$ perovskite solar cells were constructed. Furthermore, the photo-generated charge-carrier transfer from $Cs_2AgBiBr_6$ to the adjacent carrier extraction layers was systematically investigated *via* femtosecond transient spectroscopies. This study offers a new pathway to acquiring high-quality $Cs_2AgBiBr_6$ thin films and provides a useful guide toward the development of high-efficiency double perovskite solar cells in the future.

Keywords: lead-free double perovskite, solar cell, one-step spin-coating, $Cs_2AgBiBr_6$, charge transfer dynamics

INTRODUCTION

Mixed-cation lead halide perovskite solar cells have significantly progressed because of their certified power conversion efficiency (PCE), which is now at 25.2% [1]. However, their stability and toxicity are still the main challenges for their large-scale commercialization [2–7]. Three-dimensional lead-free double perovskite, namely $A_2M^IM^{III}X_6$ (A=Cs, MA; M^I=Ag, Na, K; M^{III}=Sb, Bi; X=Cl, Br, I), has drawn significant attention because of its satisfactory stability and environmental friendliness [8–12]. Recently, the $Cs_2AgBiBr_6$ has been successfully introduced into solar cells, demonstrating PCE as high as 2.51% [13]. However, this efficiency value is significantly lower than that of lead-based perovskite devices. The $Cs_2AgBiBr_6$ solar cell is still at an early stage of development. The relatively large indirect band gap (1.9 or 2.2 eV), large exciton binding energy, and poor crystalline quality of the prepared $Cs_2AgBiBr_6$ films are the main issues that limit the performance of $Cs_2AgBiBr_6$-based solar cells [14,15].

It is widely accepted that high-quality perovskite films with large grain size are crucial to achieving high-PCE solar cells. However, preparing compact $Cs_2AgBiBr_6$ thin films with large grain size has been a big challenge [16]. First, if using the typical solution method, the solubilities of bromide compounds are significantly low in most common solvents [17]. To solve this problem, $Cs_2AgBiBr_6$ single crystals were typically synthesized first and then redissolved into the solvent instead of directly dissolving CsBr, AgBr, and $BiBr_3$ to form the precursor solution. However, this complex method substantially increased the experimental time and device fabrication cost [13,17–19]. If using the thermal evaporation method, the experimental procedure is relatively simpler. However, compared with the solution method, the energy cost of device fabrication is significantly higher and the PCE of the produced cells is considerably lower [20,21]. Igbari *et al.* [13] reported that the double perovskite films pro-

Joint Key Laboratory of the Ministry of Education, Institute of Applied Physics and Materials Engineering, University of Macau, Avenida da Universidade, Taipa, Macau SAR 999078, China
[†] These authors contributed equally to this work.
[*] Corresponding author (email: gcxing@um.edu.mo)

duced by using the solution method showed better film quality, narrower electronic bandgap, longer photogenerated charge-carrier lifetime, and higher carrier mobility than those of the films deposited using the thermal evaporation method. Second, it was difficult to directly obtain the dense pinhole-free $Cs_2AgBiBr_6$ thin film *via* the conventional one-step spin coating. Although the low-pressure-assisted method [22–25] can solve this problem, it makes the process complicated. Therefore, a novel facile deposition method that could be used to produce high-quality $Cs_2AgBiBr_6$ films with large grain size is still highly desired.

For high-quality nucleation and crystal growth in spin-coated solution films, the properties of the solvents are significantly important [26]. A satisfactory solvent for spin coating should possess high dissolvability, low boiling point, and high vapor pressure [27]. Accordingly, dimethyl sulfoxide (DMSO) was typically chosen as the solvent to deposit $Cs_2AgBiBr_6$ thin films because of its high dissolvability [14,18,19,22]. However, DMSO possesses high boiling point (189°C) and low vapor pressure (0.42 mmHg at 20°C), thereby likely resulting in slow solvent evaporation during spin coating. Therefore, films with large roughness and many pinholes were typically achieved [28–30]. A facile way to address this issue is adding a low-boiling-point and high-vapor-pressure solvent into DMSO to tune the properties thereof and form a moderate solvent mixture. Accordingly, *N*,*N*-dimethylformamide (DMF) with low boiling point (153°C) and high vapor pressure (2.7 mmHg at 20°C) has been widely used as the solvent in the process of lead halide perovskite film deposition [31], and it may also satisfactorily function as the additive for $Cs_2AgBiBr_6$ thin-film deposition. Furthermore, on the basis of the pre-synthesized $Cs_2AgBiBr_6$ single crystal powder, Yang *et al.* [32] recently reported that the grain size of the deposited $Cs_2AgBiBr_6$ film could be enlarged by adding a small amount of DMF into DMSO. Herein, for the first time, a facile one-step spin-coating method is developed to prepare high-quality $Cs_2AgBiBr_6$ thin films with large grain size. The DMSO and DMF mixture is used as the solvent and chlorobenzene (CB) as the antisolvent. *Via* preheating the precursor and substrate (hot-casting), compact $Cs_2AgBiBr_6$ films with an average grain size of approximately 0.5 μm could be achieved by annealing the spin-coated film at 285°C for 5 min. Double perovskite solar cells with PCE over 1% were demonstrated with these films. In addition, the charge-carrier transfer dynamics from the $Cs_2AgBiBr_6$ film to the adjacent carrier extraction layers were systematically investigated *via* femtosecond transient absorption (TA) and time-resolved photoluminescence (TRPL) measurements. In this study, we demonstrate a facile one-step spin-coating method to deposit high-quality $Cs_2AgBiBr_6$ thin films with large grain size, and these films will advance the development of $Cs_2AgBiBr_6$ double perovskite solar cells.

EXPERIMENTAL SECTION

Materials

CsBr (99.999%) and $BiBr_3$ (99%) were purchased from Alfa Aesar. AgBr (99.9%) was purchased from Sigma-aldrich. DMF (99.8%, extra dry), DMSO (99.9%) and CB (99.8%, extra dry) were purchased from Acros. 2,2',7,7'-Tetrakis(*N*,*N*-di-*p*-methoxyphenylamine)-9,9'-spirobifluorene (Spiro-OMeTAD, 99.8%), phenyl-C_{61}-butyric acid methyl ester (PCBM, 99%), *tert*-butylpyridine (TBP 96%), and lithium bis(trifluoromethylsulphonyl)vimidev (LiTFSI, 99%) were purchased from Xi'an Polymer Light Technology Corp. Alcohol (99%) was purchased from Tianjin Fuyu Fine Chemical Co., Ltd. Acetone (analytical reagent, AR) was purchased from Sinopharm Chemical Regent Co, Ltd. SnO_2 (15% in H_2O colloidal) was purchased from Alfa Aesar. All the chemicals were used as received without further purification.

$Cs_2AgBiBr_6$ precursor preparation

CsBr (0.8 mmol; 0.1702 g), AgBr (0.4 mmol; 0.0751 g), and $BiBr_3$ (0.4 mmol; 0.1794 g) were dissolved in the solvent mixture that comprised DMSO (1 mL) and DMF (1 mL). The solution was stirred for several hours at 60–80°C until all the chemicals were dissolved.

$Cs_2AgBiBr_6$ thin film deposition and device fabrication

First, the etched indium tin oxide (ITO) glass was cleaned using deionized water, acetone, deionized water and ethanol under ultrasonic each for 10 min, and then treated under UV-ozone for 15 min. The SnO_2 electron transport layer (ETL) was deposited by spin-coating SnO_2 colloidal in deionized water (1:6, *v*/*v*) at 3000 r min^{-1} for 30 s in the air. The following operations were conducted in the glove box with oxygen (50 ppm) and H_2O (0.1 ppm). Both the prepared $Cs_2AgBiBr_6$ precursor and SnO_2-coated ITO substrate were preheated on a hot plate at 75°C for a few minutes before spin coating. Subsequently, 80 μL hot $Cs_2AgBiBr_6$ precursor was spin coated onto the hot substrate at 600 r min^{-1} for 2 s, 1500 r min^{-1} for 3 s, and 3000 r min^{-1} for 30 s. In addition, 500 μL CB as the antisolvent was dropped onto the $Cs_2AgBiBr_6$ film at approximately 10 s (i.e., at the gelation point) before

the end of the spin coating procedure. The deposited $Cs_2AgBiBr_6$ thin film was aged for 2 min in the glovebox at room temperature before annealing it at 285°C for 5 min on the hot plate. After cooling the $Cs_2AgBiBr_6$ thin film to room temperature, a Sprio-OMeTAD solution was spin coated on the top of the film at the speed of 3000 r min^{-1} for 30 s. The Sprio-OMeTAD solution was prepared by dissolving 73 mg Spiro-OMeTAD in 1 mL CB with 17.5 μL TBP and 28.5 μL LiTFSI (520 mg mL^{-1} LiTFSI in acetonitrile). Finally, 80 nm Au was evaporated on the top of the device through a shadow mask. The active area of the $Cs_2AgBiBr_6$ solar cell was 0.04 cm^2.

Characterization

X-ray diffraction (XRD) measurements were performed using the Rigaku Smart Lab 9000W system (X-ray Source: Cu Kα radiation, where λ=1.5418 Å), and the $Cs_2AgBiBr_6$ film was spin coated on a glass substrate. The scanning electron microscopy (SEM) images of the $Cs_2AgBiBr_6$ films were obtained using field-emission SEM (Zeiss Sigma) under high vacuum at the electron energy of 5 kV. UV-Vis absorption spectra were measured using a spectrophotometer (Shimadzu UV-2600). The valence band and Fermi level were measured by ultraviolet photoelectron spectroscopy (UPS; Thermo scientific, ESCALAB Xi+). The current density-voltage (*J-V*) curves were recorded using a source meter (Keithley 2400) and the simulated solar illumination was provided using a solar simulator (Newport) under AM 1.5 G at 100 mW cm^{-2} illumination. The photoluminescence (PL) and TRPL measurements were performed using 400-nm femtosecond excitation pulses, and the pulsed laser was incident from the perovskite side (quartz side) (100 fs). The 400-nm laser pulses were generated by passing the strong 800-nm femtosecond laser beam through a BBO crystal. The TA spectra of the $Cs_2AgBiBr_6$ films were measured using a spectrometer (Ultrafast HELIOS TA).

RESULTS AND DISCUSSION

Precisely controlling the nucleation and crystal growth processes during the film deposition is critical to achieving high-quality $Cs_2AgBiBr_6$ films with compact surfaces and large grain size. According to classical nucleation and growth theory, such as the LaMer model, high nucleation density facilitates the formation of uniform compact thin films [29,33]. Therefore, either a high-vapor-pressure and low-boiling-point solvent or a strategy (hot-casting, low-pressure, solvent engineering) that could accelerate the evaporation of the low-vapor-pressure and high-boiling-point solvent is desired [34]. Although having satisfactory precursor solubility, DMSO, with its high boiling point (189°C) and low vapor pressure (0.42 mmHg at 20°C) is not an ideal solvent (Table S1) for spin coating. However, DMF, with its lower boiling point (153°C), and higher vapor pressure (2.7 mmHg at 20°C), is more preferred for grain growth and high-quality $Cs_2AgBiBr_6$ film deposition. Therefore, in this study, the DMSO and DMF mixture is used as the solvent instead of the generally used DMSO to deposit the $Cs_2AgBiBr_6$ films (Table S1). The deposition process is depicted in Fig. 1. Without pre-synthesizing the $Cs_2AgBiBr_6$ single crystal powder, CsBr, AgBr, and $BiBr_3$ were directly dissolved in the DMSO and DMF mixture and stirred at 80°C. The maximum dissolving concentration of $Cs_2AgBiBr_6$ is 0.4 mol L^{-1} in the optimized solvent mixture (V_{DMSO}/V_{DMF}=1:1). The $Cs_2AgBiBr_6$ solubility decreased upon increasing the volume ratio of DMF (Table S2). As shown in Fig. S1, the totally dissolved $Cs_2AgBiBr_6$ precursor solution is yellow. Before spin coating, the precursor solution and substrates were preheated at 75°C, as this could accelerate the solvent evaporation and result in higher nucleation density. Furthermore, CB was used as the antisolvent during the spin coating to quickly extract the solvent, and, consequently, the nucleation density in the film rapidly increased [35]. Without low-pressure assistance, the as-prepared $Cs_2AgBiBr_6$ thin films were aged for 2 min at room temperature and then annealed at 285°C for 5 min, and this is an important step to obtain large-grain-size films after gaining the as-prepared $Cs_2AgBiBr_6$ thin films. According to the Ostwald ripening process, the aging and post-annealing process is essential for the grain growth

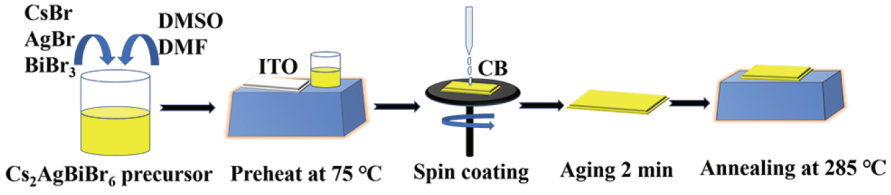

Figure 1 Deposition process of the $Cs_2AgBiBr_6$ thin film.

[29]. Using the above-mentioned facile one-step spin-coating method, the nucleation and crystal growth of $Cs_2AgBiBr_6$ can be precisely controlled. Compact double perovskite films with an average grain size of approximately 0.5 μm were achieved.

First, the effect of the DMF volume ratio in the solvent mixture on the $Cs_2AgBiBr_6$ thin film deposition was investigated. In Fig. S2, we depict the top-view SEM images of the films deposited using solutions with various DMSO-to-DMF volume ratios (without the antisolvent CB). From Fig. S2a, it is evident that the film possesses a significant number of pinholes without DMF. The pinhole size and density decrease upon increasing the DMF volume ratio in the solvent mixture (Fig. S2). From the results, it is confirmed that quick evaporation of the solvent can increase the nucleation density in the spin-coated film. However, even upon increasing the volume ratio of DMF to 50%, the deposited $Cs_2AgBiBr_6$ film is still not perfect and possesses several pinholes (Fig. S2f). Accordingly, to further improve the film quality, CB was utilized as the antisolvent. In Fig. S3, we depict the SEM images of the films deposited using the solvent mixture and antisolvent CB. From both Fig. S2 and these results, it is evident that significantly more compact and smoother $Cs_2AgBiBr_6$ films could be achieved using the CB treatment for all the DMSO-to-DMF volume ratios. A near pinhole free and compact double perovskite film with the average gain size of approximately 0.5 μm was achieved under the condition of using 1:1 volume ratio solvent and CB antisolvent (Fig. S3f). The atomic force microscopy (AFM) images further confirmed the perfectness of the films with significantly small surface roughness (Fig. S4). In addition, the effect of different aging times at room temperature on the prepared $Cs_2AgBiBr_6$ thin films was investigated. As shown in Fig. S5, the grain size first slightly increased and the pinhole density decreased upon increasing the aging time. However, if the aging time was increased to over 3 min, some small pinholes would reappear again. Here, the phenomenon of pinhole changes during the aging process can be explained using the Ostwald ripening process. During the aging process, the residual solvent evaporates further in the as-deposited thin film, increasing both the concentration of the nucleation and grain size. Therefore, a dense thin film is formed with large grains and negligible number of pinholes. However, upon increasing the aging time to over 3 min, a few of the large grains grow significantly large and some grains are considerably small, resulting in the ununiform distribution of grain sizes and also the pinholes increase again.

After optimizing the film deposition process, a high-quality $Cs_2AgBiBr_6$ thin film with large grain sizes was achieved, as depicted in Fig. 2a. The XRD pattern of the film prepared in optimized experimental conditions is depicted in Fig. 2b. The recorded peaks matched well with the simulated ones of $Cs_2AgBiBr_6$. This consistency confirmed that the dominant component in the film is the crystallized $Cs_2AgBiBr_6$. The linear absorption of the prepared double perovskite film is shown in Fig. 2c. A clear sharp absorption peak is located at 438 nm, and it could be attributed to the exciton absorption in $Cs_2AgBiBr_6$ [36–38]. Such sharp excitonic absorption indicates enormous exciton binding energy within this double perovskite. The indirect band gap value determined using the absorption spectra is approximately 2.15 eV (Fig. S6). The absorption coefficient of the film measured at 440 nm is approximately 1.18×10^5 cm^{-1}, which is comparable to the absorption values reported for lead-based perovskites for most visible wavelengths [39,40]. The large light-absorption coefficient suggests satisfactory photon harvesting potential when the incident photon energy is greater than the band gap. In Fig. 2d, we depict the steady-state PL spectrum of the $Cs_2AgBiBr_6$ thin film pumped at 400 nm. Because of the intrinsic indirect band gap, the broad near white light PL should originate from trap state emission, which typically possesses a significantly low quantum yield. However, the measured defect state emission in $Cs_2AgBiBr_6$ is significantly stronger than that observed in lead-based perovskites under the same experimental conditions [32]. This result suggests that the deposited $Cs_2AgBiBr_6$ film still possesses significantly higher trap states than those of

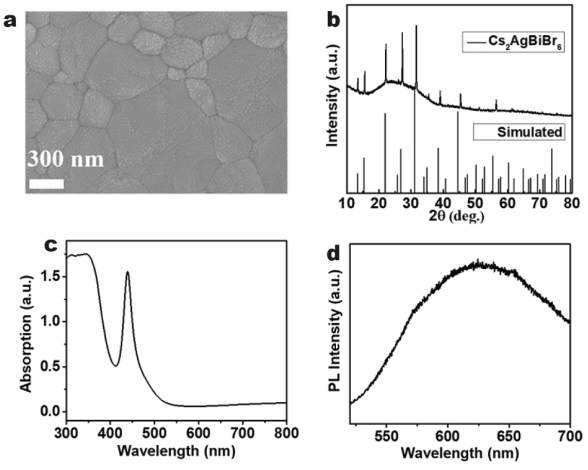

Figure 2 Characterizations of the $Cs_2AgBiBr_6$ thin film. (a) The top-view SEM image; (b) the XRD pattern; (c) the optical absorption; (d) the PL spectrum upon excitation at 400 nm (100 fs, 1 kHz).

the typical lead-based perovskite films.

To construct an efficient photovoltaic device, a satisfactory energy alignment is essential. Therefore, the band structure and Fermi level of the deposited $Cs_2AgBiBr_6$ thin film were characterized *via* UPS. The results are shown in Fig. 3a, b. The Fermi level was calculated as E_f=21.22–E_{cutoff}, where E_f denotes the Fermi level, and E_{cutoff} denotes the high binding energy cutoff [41]. The valence band was obtained as E_{VB}=E_f+E_0, where E_0 denotes the low bonding energy tail, and E_{VB} denotes the valence band [42]. The calculated values of E_{VB} and E_f are −5.92 and −5.14 eV, respectively. The conduction band was extracted from the band gap E_g of the $Cs_2AgBiBr_6$ thin film (Fig. S6) and calculated as E_{CB}=E_{VB}+E_g. Its value is −3.77 eV.

On the basis of the band structure of the prepared $Cs_2AgBiBr_6$ film, SnO_2 was chosen as ETL and Spiro-OMeTAD as the hole transport layer (HTL) to construct the solar cell device. The corresponding energy alignment diagram is depicted in Fig. 3c. Subsequently, the complete device was fabricated on the basis of the structure of ITO/SnO_2/$Cs_2AgBiBr_6$/Spiro-OMeTAD/Au, as depicted in Fig. 3d. The best-performing device showed a PCE of 1.11%. The corresponding *J-V* curves measured under AM 1.5 G and dark environment are presented in Fig. 3e. Negligible hysteresis was observed for this double perovskite device (Fig. S7), likely indicating that the ion migration and interfacial charge transfer barrier are not as significant as those observed in some lead-based devices. In addition, the $Cs_2AgBiBr_6$ solar cell showed satisfactory reproducibility (Fig. S8). The typical cross-section SEM image of the device is shown in the inset of Fig. 3e. The picture clearly shows that large $Cs_2AgBiBr_6$ grains are present throughout the absorber layer. From these results, it is further confirmed that high-quality double perovskite films can be deposited using the facile one-step spin-coating method.

We next investigated the charge-transfer kinetics between the perovskite and charge extraction layers. Pristine $Cs_2AgBiBr_6$, $Cs_2AgBiBr_6$/PCBM and $Cs_2AgBiBr_6$/Spiro-OMeTAD films were deposited on quartz for PL and TRPL measurements (see Fig. 4a, b). As shown in Fig. 4a, all the PL intensities are observable but weak for the low trap state emission quantum yield. This result indicates that substantial photon-injected charge carriers will be localized to the trap states below band gap. However, strangely, the HTL layer (Spiro-OMeTAD layer) could extract carriers significantly more efficiently from the trap states than the ETL layer (PCBM). To further study this result, TRPL measurements were also conducted (Fig. 4b). The results are consistent with the PL study, confirming that the quenching ability of Spiro-OMeTAD is better than that of PCBM. The TRPL-curves fitted data are summarized in Table S3. The lifetime τ_{eff} (i.e., the time at which the PL intensity drops to 1/e of its maximum value) of the $Cs_2AgBiBr_6$ pristine film is 18.2 ns. However, upon coating Spiro-OMeTAD and PCBM onto the $Cs_2AgBiBr_6$ film, the PL intensity quickly decayed, resulting in the lifetimes of 7.4 and 15.1 ns, respectively. In addition, extracted from the TRPL quenching, the hole diffusion length of the $Cs_2AgBiBr_6$ film could reach over 110 nm [18], and the photoexcitation mobility could reach 0.8 $cm^2 V^{-1} s^{-1}$, both of which are comparable to the values reported for lead halide

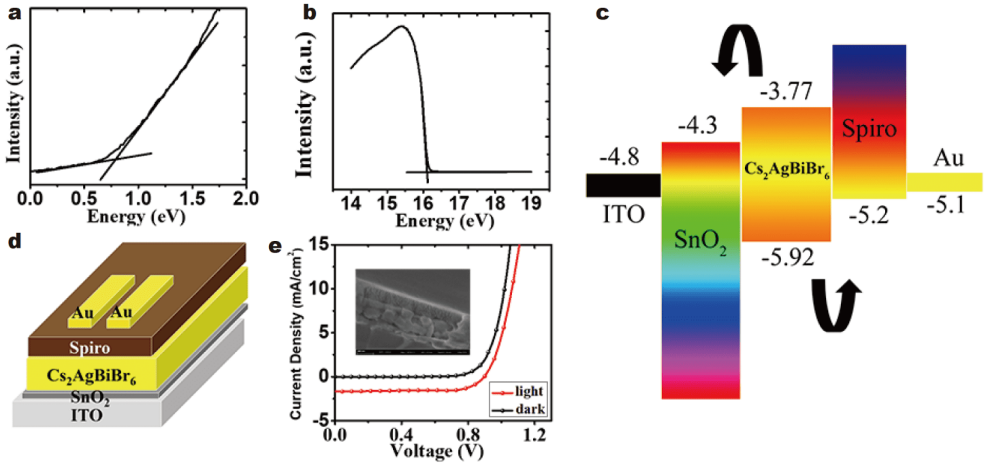

Figure 3 (a, b) The UPS spectra of the $Cs_2AgBiBr_6$ thin film; (c) the energy alignment diagram; (d) the device-configuration diagram; (e) *J-V* curves measured under AM 1.5 G and dark conditions (inset: cross-section SEM image of the device).

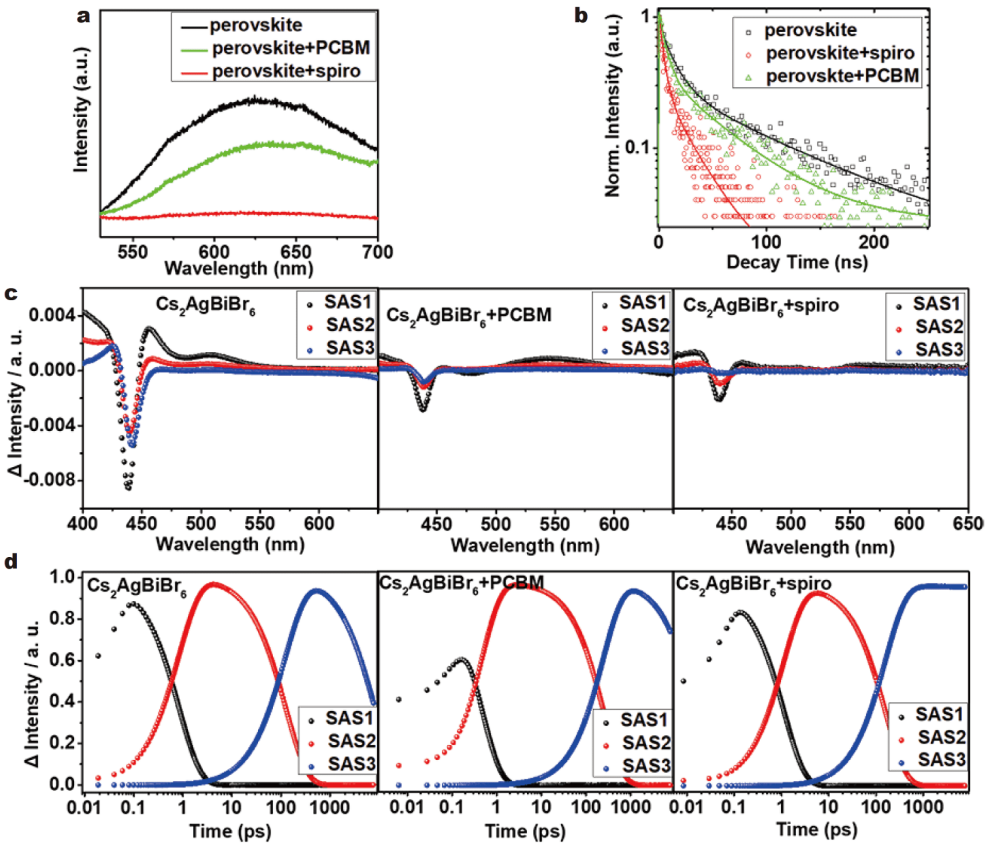

Figure 4 Charge-carrier dynamics. (a) PL spectra; (b) normalized TRPL spectra; (c) deconvoluted species associated spectra of $Cs_2AgBiBr_6$, $Cs_2AgBiBr_6$/PCBM, and $Cs_2AgBiBr_6$/Spiro-OMeTAD (the samples were photo-excited at 350 nm (100 fs, 1 kHz)); (d) the population dynamics of $Cs_2AgBiBr_6$, $Cs_2AgBiBr_6$/PCBM, and $Cs_2AgBiBr_6$/Spiro-OMeTAD.

perovskites. However, for electron extraction, the electron diffusion length of the $Cs_2AgBiBr_6$ film was only approximately 50 nm and the mobility approximately 0.2 $cm^2 V^{-1} s^{-1}$.

The TA spectroscopy was conducted to further study the deactivation process (Fig. 4c). Similar absorption features at approximately 420, 460, and 520 nm due to photo-induced absorption and at 440 nm for exciton absorption bleach were noticed. Furthermore, global analysis was applied using a three-species sequential model. Their corresponding species-associated spectra (SAS) and relative population dynamics are provided in Fig. 4d. In the case of $Cs_2AgBiBr_6$, the electron population happens in the femtosecond scale, followed by the quick relaxation by charge-carrier trapping and carrier-carrier scattering within 1 ps. Subsequently, two more carrier relaxation stages were noticed with the lifetimes of 126 ps and 8.2 ns (Table S4). The longer lifetime in the nanosecond scale should correspond to the electron-hole recombination. Interestingly, this lifetime in $Cs_2AgBiBr_6$/PCBM reached 2047 ns compared with that of only 27 ns in the case of $Cs_2AgBiBr_6$/Spiro-OMeTAD (Table S4). Additionally, from the spectra of $Cs_2AgBiBr_6$/PCBM in Fig. 4c, it is evident that PCBM has been populated as well with the characteristic singlet excited state absorption feature around 550 nm. Unfortunately, due to the low resolution of the TA results in the first picosecond, it is not possible to separate its signal further. However, by tracing this signal, the absence of its triplet excited signal strongly indicates its participation in the charge separation process. Energetically, a mismatch of the energy alignment between the $Cs_2AgBiBr_6$ perovskite layer and the ETL or HTL layer should make a difference for this phenomenon. To confirm it, SnO_2 was chosen as a reference. Consistent with our speculation and different with $Cs_2AgBiBr_6$/PCBM, the $Cs_2AgBiBr_6$ film on SnO_2 demonstrates strong PL quenching (Fig. S9a) with a normal lifetime of approximately 11 ns (Fig. S10). For the schematic of the energy alignment diagram of PCBM and SnO_2, please see Fig. S9b. Therefore, instead of PCBM,

SnO_2 is chosen as the ETL in the $Cs_2AgBiBr_6$ solar cell device.

CONCLUSIONS

In summary, a facile one-step spin-coating method was developed to deposit high-quality $Cs_2AgBiBr_6$ film with large grain sizes. The nucleation and crystal growth of $Cs_2AgBiBr_6$ could be precisely controlled by using the DMSO-DMF mixture as the solvent and CB as the anti-solvent and *via* post annealing at an appropriately high temperature. Compact double perovskite films with an average grain size of approximately 0.5 μm could be achieved. On the basis of these films, satisfactory high-efficiency double perovskite solar cells were constructed with the device structure of ITO/SnO_2/$Cs_2AgBiBr_6$/Spiro-OMeTAD/Au. In addition, the photo-generated charge-carrier transfer dynamics from $Cs_2AgBiBr_6$ to the adjacent carrier extraction layers were systematically investigated. This study offers a new pathway to acquiring high-quality $Cs_2AgBiBr_6$ thin films and provides a useful guide toward the development of high-efficiency double perovskite solar cells in the future.

Received 23 February 2020; accepted 12 April 2020; published online 25 May 2020

1 Best research-cell efficiencies (NREL). https://www.nrel.gov/pv/assets/pdfs/best-research-cell-efficiencies.20200203.pdf, (accessed: Februay 2020)
2 Rong Y, Hu Y, Mei A, *et al.* Challenges for commercializing perovskite solar cells. Science, 2018, 361: eaat8235
3 Correa-Baena JP, Saliba M, Buonassisi T, *et al.* Promises and challenges of perovskite solar cells. Science, 2017, 358: 739–744
4 Hu H, Dong B, Zhang W. Low-toxic metal halide perovskites: opportunities and future challenges. J Mater Chem A, 2017, 5: 11436–11449
5 Igbari F, Wang Z, Liao L. Progress of lead-free halide double perovskites. Adv Energy Mater, 2019, 9: 1803150
6 Liang C, Zhao D, Li Y, *et al.* Ruddlesden-popper perovskite for stable solar cells. Energy Environ Mater, 2018, 1: 221–231
7 Zhang B, Lei Y, Qi R, *et al.* An *in-situ* room temperature route to $CuBiI_4$ based bulk-heterojunction perovskite-like solar cells. Sci China Mater, 2018, 62: 519–526
8 Pan W, Wu H, Luo J, *et al.* $Cs_2AgBiBr_6$ single-crystal X-ray detectors with a low detection limit. Nat Photon, 2017, 11: 726–732
9 Slavney AH, Hu T, Lindenberg AM, *et al.* A bismuth-halide double perovskite with long carrier recombination lifetime for photovoltaic applications. J Am Chem Soc, 2016, 138: 2138–2141
10 Tran TT, Panella JR, Chamorro JR, *et al.* Designing indirect-direct bandgap transitions in double perovskites. Mater Horiz, 2017, 4: 688–693
11 Zhang C, Gao L, Teo S, *et al.* Design of a novel and highly stable lead-free Cs_2NaBiI_6 double perovskite for photovoltaic application. Sustain Energy Fuels, 2018, 2: 2419–2428
12 Luo J, Wang X, Li S, *et al.* Efficient and stable emission of warm-white light from lead-free halide double perovskites. Nature, 2018, 563: 541–545
13 Igbari F, Wang R, Wang ZK, *et al.* Composition stoichiometry of $Cs_2AgBiBr_6$ films for highly efficient lead-free perovskite solar cells. Nano Lett, 2019, 19: 2066–2073
14 Greul E, Petrus ML, Binek A, *et al.* Highly stable, phase pure $Cs_2AgBiBr_6$ double perovskite thin films for optoelectronic applications. J Mater Chem A, 2017, 5: 19972–19981
15 Du KZ, Meng W, Wang X, *et al.* Bandgap engineering of lead-free double perovskite $Cs_2AgBiBr_6$ through trivalent metal alloying. Angew Chem Int Ed, 2017, 56: 8158–8162
16 Kung PK, Li MH, Lin PY, *et al.* Lead-free double perovskites for perovskite solar cells. Sol RRL, 2019, 4: 1900306
17 Gao W, Ran C, Xi J, *et al.* High-quality $Cs_2AgBiBr_6$ double perovskite film for lead-free inverted planar heterojunction solar cells with 2.2 % efficiency. ChemPhysChem, 2018, 19: 1696–1700
18 Pantaler M, Cho KT, Queloz VIE, *et al.* Hysteresis-free lead-free double-perovskite solar cells by interface engineering. ACS Energy Lett, 2018, 3: 1781–1786
19 Ning W, Wang F, Wu B, *et al.* Long electron-hole diffusion length in high-quality lead-free double perovskite films. Adv Mater, 2018, 30: 1706246
20 Wang M, Zeng P, Bai S, *et al.* High quality sequential vapor deposited $Cs_2AgBiBr_6$ thin films for lead-free perovskite solar cells. Sol RRL, 2018, 2: 1800217
21 Fan P, Peng HX, Zheng ZH, *et al.* Single-source vapor-deposited $Cs_2AgBiBr_6$ thin films for lead-free perovskite solar cells. Nanomaterials, 2019, 9: 1760
22 Wu C, Zhang Q, Liu Y, *et al.* The dawn of lead-free perovskite solar cell: highly stable double perovskite $Cs_2AgBiBr_6$ film. Adv Sci, 2018, 5: 1700759
23 Zhang Z, Wu C, Wang D, *et al.* Improvement of $Cs_2AgBiBr_6$ double perovskite solar cell by rubidium doping. Org Electron, 2019, 74: 204–210
24 Li Y, Shi Z, Lei L, *et al.* Ultrastable lead-free double perovskite photodetectors with imaging capability. Adv Mater Interfaces, 2019, 6: 1900188
25 Lei LZ, Shi ZF, Li Y, *et al.* High-efficiency and air-stable photodetectors based on lead-free double perovskite $Cs_2AgBiBr_6$ thin films. J Mater Chem C, 2018, 6: 7982–7988
26 Ren Y, Duan B, Xu Y, *et al.* New insight into solvent engineering technology from evolution of intermediates *via* one-step spin-coating approach. Sci China Mater, 2017, 60: 392–398
27 Todorov T, Mitzi DB. Direct liquid coating of chalcopyrite light-absorbing layers for photovoltaic devices. Eur J Inorg Chem, 2010, 2010(1): 17–28
28 Thanh NTK, Maclean N, Mahiddine S. Mechanisms of nucleation and growth of nanoparticles in solution. Chem Rev, 2014, 114: 7610–7630
29 Dunlap-Shohl WA, Zhou Y, Padture NP, *et al.* Synthetic approaches for halide perovskite thin films. Chem Rev, 2018, 119: 3193–3295
30 Jung M, Ji SG, Kim G, *et al.* Perovskite precursor solution chemistry: from fundamentals to photovoltaic applications. Chem Soc Rev, 2019, 48: 2011–2038
31 Luo D, Yang W, Wang Z, *et al.* Enhanced photovoltage for inverted planar heterojunction perovskite solar cells. Science, 2018, 360: 1442–1446
32 Yang J, Bao C, Ning W, *et al.* Stable, high-sensitivity and fast-response photodetectors based on lead-free $Cs_2AgBiBr_6$ double

perovskite films. Adv Opt Mater, 2019, 7: 1801732
33 Pascoe AR, Gu Q, Rothmann MU, *et al.* Directing nucleation and growth kinetics in solution-processed hybrid perovskite thin-films. Sci China Mater, 2017, 60: 617–628
34 Liu T, Zhou Y, Hu Q, *et al.* Fabrication of compact and stable perovskite films with optimized precursor composition in the fast-growing procedure. Sci China Mater, 2017, 60: 608–616
35 Jeon NJ, Noh JH, Kim YC, *et al.* Solvent engineering for high-performance inorganic–organic hybrid perovskite solar cells. Nat Mater, 2014, 13: 897–903
36 Steele JA, Pan W, Martin C, *et al.* Photophysical pathways in highly sensitive $Cs_2AgBiBr_6$ double-perovskite single-crystal X-ray detectors. Adv Mater, 2018, 30: 1804450
37 Schade L, Wright AD, Johnson RD, *et al.* Structural and optical properties of $Cs_2AgBiBr_6$ double perovskite. ACS Energy Lett, 2018, 4: 299–305
38 Kentsch R, Scholz M, Horn J, *et al.* Exciton dynamics and electron-phonon coupling affect the photovoltaic performance of the $Cs_2AgBiBr_6$ double perovskite. J Phys Chem C, 2018, 122: 25940–25947
39 Xing G, Mathews N, Sun S, *et al.* Long-range balanced electron- and hole-transport lengths in organic-inorganic $CH_3NH_3PbI_3$. Science, 2013, 342: 344–347
40 Zhang Z, Sun F, Zhu Z, *et al.* Unconventional solution-phase epitaxial growth of organic-inorganic hybrid perovskite nanocrystals on metal sulfide nanosheets. Sci China Mater, 2018, 62: 43–53
41 Chen W, Wu Y, Yue Y, *et al.* Efficient and stable large-area perovskite solar cells with inorganic charge extraction layers. Science, 2015, 350: 944–948
42 Zhao D, Wu Y, Tu B, *et al.* Understanding the impact of Cu-In-Ga-S nanoparticles compactness on holes transfer of perovskite solar cells. Nanomaterials, 2019, 9: 286

Acknowledgements The authors acknowledge financial support from Macau Science and Technology Development Fund (FDCT-116/2016/A3, FDCT-091/2017/A2 and FDCT-014/2017/AMJ), the Research Grants (SRG2016-00087-FST, MYRG2018-00148-IAPME) from University of Macau, the National Natural Science Foundation of China (91733302, 61605073, 61935017), and the Natural Science Foundation of Guangdong Province, China (2019A1515012186).

Author contributions Zhao D and Xing G conceived the idea. Zhao D conducted the experiments. All authors contributed to the date analysis and co-drafted the manuscript. Xing G led the project.

Conflict of interest The authors declare that they have no conflict of interest.

Supplementary information Supporting data are available in the online version of the paper.

Dandan Zhao graduated from Henan University with master degree, focusing on the solution-processed copper indium gallium selenide ($CuIn_xGa_{(1-x)}Se_2$) thin film solar cells. She is currently a PhD candidate in the Institute of Applied Physics and Materials Engineering (IAPME) at University of Macau under the supervision of Professor Guichuan Xing, and has interests in using the lead-free perovskite materials to fabricate stable solar cells.

Bingzhe Wang received his master degree in material engineering in 2014 from Qingdao University of Science and Technology, where he received his BSc degree. In 2019, he received his PhD degree in physical chemistry from the Friedrich-Alexander University of Erlangen-Nuremberg. He is currently a postdoctoral researcher in the IAPME, University of Macau. His research interest focus on ultrafast carrier dynamics in solar energy conversion.

Chao Liang graduated with a BSc degree from Henan University of Technology (2014) as well as a MSc degree in materials science from Zhengzhou University (2017). He is currently a PhD candidate in the IAPME at University of Macau under the supervision of Professor Guichuan Xing. His research areas focus on perovskite solar cells and quantum dot solar cells.

Guichuan Xing obtained his BSc degree in light sources and illuminating engineering from Fudan Univesity in 2003 and PhD in physics from the National University of Singapore in 2011. He joined the IAPME, University of Macau as an assistant professor in 2016. His current research interests include nonlinear optical properties and ultrafast carrier dynamics in novel optoelectronic materials and devices.

高效制备优质$Cs_2AgBiBr_6$薄膜及其太阳能电池

赵丹丹[†], 王冰哲[†], 梁超[†], 刘堂昊, 魏琪, 王思思, 王开阳, 张志鹏, 李晓军, 彭少敏, 邢贵川[*]

摘要 无铅双钙钛矿$Cs_2AgBiBr_6$与铅基钙钛矿相比具有更高的稳定性和更低的毒性，被认为是很有前途的下一代光伏材料．在实际应用中，人们迫切需要一种简便的沉积方法来制备高质量、大晶粒尺寸的双钙钛矿薄膜．然而，目前尚未找到制备$Cs_2AgBiBr_6$薄膜的简便方法．本文通过简单的一步旋涂法成功制备了晶粒尺寸达0.5 μm的高质量$Cs_2AgBiBr_6$薄膜，该方法使用体积比优化后的二甲基亚砜-二甲基甲酰胺(DMSO-DMF)混合溶液作为溶剂，氯苯作为反溶剂．基于良好的薄膜质量，制备了高效(>1%)$Cs_2AgBiBr_6$钙钛矿太阳能电池．此外，利用飞秒瞬态光谱系统地研究了$Cs_2AgBiBr_6$与相邻的载流子传输层之间的光生电荷转移．本工作为制备高质量的$Cs_2AgBiBr_6$薄膜开辟了新方法，为高效双钙钛矿太阳能电池的发展提供了有益指导．

